Neutron diffraction study of the magnetic (H,T) phase diagrams of $EuAs_3$ and $Eu(As_{1-x}P_x)_3$

T. Chattopadhyay
Département de Recherche Fondamentale, Service de Physique, Groupe Magnétisme et Diffraction Neutronique, Centre d'Etudes Nucléaires de Grenoble, Boîte Postale No. 85X, 38041 Grenoble Cedex, France

P. J. Brown
Institut Laue-Langevin, Boîte Postale No. 156X, 38042 Grenoble Cedex, France
(Received 23 December 1987)

The magnetic (H,T) phase diagrams of $EuAs_3$ and $Eu(As_{1-x}P_x)_3$ for $x=0.10$, 0.40, 0.80, and 0.98 with the applied magnetic field parallel to the monoclinic b axis of the crystals have been investigated using neutron diffraction. These phase diagrams contain several commensurate and incommensurate phases which are unexpected for a single Eu^{2+} ion in the $^8S_{7/2}$ ground state. The temperature and field variations of the wave vectors and the magnetic structures of the field-induced phases have been determined. Phase transitions between these phases are discussed in terms of phenomenological Landau-type theory and symmetry arguments.

I. INTRODUCTION

Semimetallic $EuAs_3$ and its solid solution $Eu(As_{1-x}P_x)_3$ have rather complex magnetic properties unexpected for the Eu^{2+} ion in the $^8S_{7/2}$ ground state.[1-9] $EuAs_3$ orders at $T_N=11.3$ K with a second-order phase transition to a sine-wave amplitude-modulated incommensurate phase.[3] At $T_L=10.3$ K, $EuAs_3$ undergoes a lock-in transition to a commensurate phase.[3] An external magnetic field applied parallel to the monoclinic b axis of the crystal induces several commensurate-incommensurate phase transitions.[2] The magnetic (H,T) phase diagram of $EuAs_3$ is rather complex and contains at least six phases. The magnetic ordering in $EuAs_3$ can only be explained by assuming an anisotropic exchange interaction whose microscopic origin is not understood at the present time. The magnetic phase diagram of the arsenic-rich $Eu(As_{1-x}P_x)_3$ is very similar to that of $EuAs_3$, whereas that of the phosphorus-rich $Eu(As_{1-x}P_x)_3$ is very different. At zero applied magnetic field phosphorus-rich $Eu(As_{1-x}P_x)_3$ orders with a sine-wave incommensurate phase at T_N.[9] At lower temperature the phosphorus-rich $Eu(As_{1-x}P_x)_3$ undergoes a sine wave to helimagnetic phase transition.[9] The magnetic (H,T) phase diagram of the phosphorus-rich $Eu(As_{1-x}P_x)_3$ contains four phases which are all incommensurate. Galvanomagnetic measurements[6] have established that the charge carrier density of $Eu(As_{1-x}P_x)_3$ decreases rapidly with increasing phosphorus concentration. It is therefore natural to conclude that the difference in the magnetic properties of the arsenic-rich and the phosphorus-rich $Eu(As_{1-x}P_x)_3$ is correlated with the charge carrier concentration. In an attempt to understand the complex magnetic properties of $EuAs_3$ and $Eu(As_{1-x}P_x)_3$ and the role of charge carrier concentration on these properties, we have undertaken neutron diffraction investigations of the magnetic phase diagrams and the structures of the ordered magnetic phases. The magnetic structures of the zero-field phases of $EuAs_3$ and $Eu(As_{1-x}P_x)_3$ have already been determined.[1,3,7,9] The magnetic (H,T) phase diagram of $EuAs_3$ and the magnetic structures of the field-induced phases have been reported.[2,5] In the present investigation we have determined the magnetic structures of the field-induced phases of the arsenic-rich ($x=0$, 0.10, and 0.40) and the phosphorus-rich ($x=0.80$ and 0.98) $Eu(As_{1-x}P_x)_3$. We have also investigated the temperature and magnetic-field-induced commensurate-incommensurate phase transitions in these compounds.

This paper is organized in the following way: Sec. II is devoted to the experimental details. Section III describes the structure model of the field-induced phases of $EuAs_3$ and $Eu(As_{1-x}P_x)_3$. Sections IV–VI describe the results of neutron diffraction experiments on these compounds. In Sec. VII we describe the resulting magnetic (H,x) phase diagram, discuss the sine-wave and helimagnetic phases of this phase diagram and phase transitions between these phases in terms of phenomenological Landau-type theory and symmetry arguments. Finally, in Sec. VIII, we give the summary and main conclusions from the present investigations.

II. EXPERIMENTAL PROCEDURE

$EuAs_3$ and $Eu(As_{1-x}P_x)_3$ were synthesized from the elements using Eu of 99.9% purity and As and P of 99.999% purity as starting materials. Large single crystals of dimensions of a few cm were grown by the Bridgman technique. The composition x of $Eu(As_{1-x}P_x)_3$ was determined by atomic emission spectroscopy with an accuracy of $\pm 1\%$.

Neutron diffraction measurements were performed using the D15 diffractometer of the Institut Laue-Langevin in Grenoble. The diffractometer was used in normal beam geometry at a neutron wavelength $\lambda=1.174$ Å. Single crystals typically of size $1\times1\times5$ mm^3 with the largest dimension parallel to the b axis were used. The

crystal needle axis was fixed parallel to the ω axis of the diffractometer to reduce the effect of the strong absorption of the natural Eu in the crystal. A cryostat with a superconducting magnet capable of generating magnetic fields up to 4.6 T was used for the experiment. The temperature stability was better than ± 0.05 K in the temperature range 2 K $\leq T \leq 12$ K.

III. MAGNETIC STRUCTURES OF THE FIELD-INDUCED PHASES OF $EuAs_3$ AND $Eu(As_{1-x}P_x)_3$

The magnetic structures of the field-induced phases of $EuAs_3$ and $Eu(As_{1-x}P_x)_3$ can be described as elliptic cone structures. In these structures the magnetic moment on the europium atom whose position is given by the vector $l+\mathbf{r}_i$ (l is a lattice vector and $\mathbf{r}_i$ the position of the ith atom in the unit cell with respect to the unit cell origin) is

$$\mathbf{M}_{li}=\hat{\mathbf{u}}S_x\cos(\tau\cdot l+\varphi_i)+\hat{\mathbf{v}}S_y\sin(\tau\cdot l+\varphi_i)+\hat{\mathbf{w}}S_z \ . \quad (1)$$

In this equation τ is the propagation vector, $\hat{\mathbf{w}}$ is a unit vector parallel to the applied field direction [010], and S_z is the component of magnetic moment parallel to the field; S_z has not been measured in the neutron diffraction experiments. $\hat{\mathbf{u}}$ and $\hat{\mathbf{v}}$ are orthogonal unit vectors in the (010) plane, we have chosen their orientation so that $S_x \geq S_y$ and the direction $\hat{\mathbf{u}}$ is inclined at an angle α to $\mathbf{a}^*$ measured towards $[00\bar{1}]$. In $EuAs_3$ there are two Eu atoms in a primitive unit cell, they are related to one another by a center of symmetry at the origin. If this pair of atoms are at positions $\mathbf{r}_1$ and $\mathbf{r}_2$ with $\mathbf{r}_1=-\mathbf{r}_2$ then for all the magnetic phases $\varphi_1=\varphi_2$ so that this pair of atoms have parallel moment directions. For each structure we have obtained the values of α and $\gamma=S_y/S_x$ by a least-squares fit of the measured intensities to this model.

IV. MAGNETIC (H,T) PHASE DIAGRAM OF $EuAs_3$

The magnetic (H,T) phase diagram of $EuAs_3$ obtained with the applied magnetic field parallel to the monoclinic b axis of the crystal has already been reported.[2,4,5] Figure 1 shows the magnetic (H,T) phase diagram of $EuAs_3$ of Ref. 4 obtained from the magnetization measurements along with the present neutron diffraction results. The phase boundaries deduced from the two types of measurement agree closely. However, the magnetization experiments were not sensitive enough to determine the effect of the magnetic field on the incommensurate (IC) phase of $EuAs_3$. In the present neutron experiment we have investigated this. Figure 2 shows the intensity of the 0.915,0,−0.30 satellite reflection of the incommensurate phase of $EuAs_3$ as a function of the magnetic field applied parallel to **b**. The intensity of this reflection decreases abruptly at the critical field $H_c=0.83$ T. At about the same magnetic field the intensity of the 0.865,0,−0.195 reflection corresponding to the field-induced SF4 (spin-flop) phase increases. The magnetic

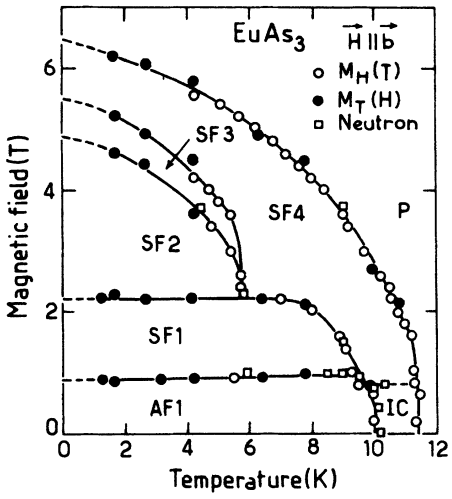

FIG. 1. The magnetic (H,T) phase diagram of $EuAs_3$ obtained from magnetization (Ref. 8) and neutron diffraction with the magnetic field applied parallel to the monoclinic b axis of the crystal.

moments of the Eu atoms in the incommensurate IC phase[3] are oriented parallel to **b**, whereas the antiferromagnetic component of the magnetic moments in the SF4 phase[2,5] are oriented parallel to **c**. Therefore, at $T=10.36$ K, $EuAs_3$ undergoes a field-induced spin-flop transition at $H_c=0.83$ T in which the magnetic moments reorient from the [010] to the [001] direction. The present experiments do not permit a definite conclusion about the order of this phase transition.

The magnetic structures of the field-induced SF1, SF2, and SF4 phases have already been reported[2,5] and are summarized in Table I. SF1 and SF4 are incommensu-

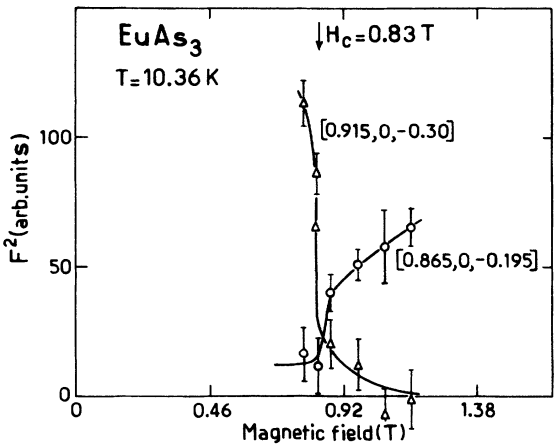

FIG. 2. Field variation of the intensities of the satellite reflections 0.915,0,−0.30 and 0.865,0,−0.915 corresponding to IC and SF4 phases of $EuAs_3$ at $T=10.36$ K illustrating field-induced IC→SF4 phase transition at $H_c=0.83$ T.

TABLE I. The magnetic structures of the field-induced phases of $EuAs_3$. α is the angle between $\mathbf{a}^*$ axis and the major axis S_x of the ellipse. S_x and S_y are the components of the magnetic moments along the major and minor axes of the ellipse, respectively. N is the number of independent reflections and R is the agreement factor between the observed and calculated structure factors.

Compound	Phase	T (K)	H (T)	Wave vector	α (deg)	S_x (μ_B)	S_y (μ_B)	N	R	Reference
$EuAs_3$	SF1	4	1.25	$(-0.9,0,0.25)$	90	5.3	4.6	42	0.15	5
$EuAs_3$	SF2	4	2.4	$(-1,0,0.25)$	90	7.6		58	0.14	5
$EuAs_3$	SF3	4	4	$(-0.95,0,0.225)$	90	5.1		55	0.14	5
$EuAs_3$	SF4	6.9	4	$(-0.9,0,0.213)$	90	3.8		34	0.13	5
$EuAs_3$	SF4	6.0	4.0	$(-0.898,0,0.213)$	98(1)	4.6(1)		31	0.13	Present work

rate phases, whereas SF2 is a commensurate phase with the wave vector $(-1,0,\frac{1}{4})$. We have determined the temperature variation of the components h and l of the wave vector parallel to $\mathbf{a}^*$ and $\mathbf{c}^*$, respectively, at different magnetic fields. Figure 3 shows these variations at $H=1.47$, 3.68, and 4.60 T. At $H=1.47$ T, the components h and l of the wave vector remain practically constant in the SF1 phase. At about $T=9$ K, h and l decrease considerably showing the phase transition from the SF1 to the SF4 phase. At $H=3.68$ T the components h and l decrease abruptly at the SF2→SF3 phase boundary at $T=4.5$ K. The SF3→SF4 transition is less evident from the temperature variation of the components of the wave vector. The temperature variation of the intensity of the satellite reflection $\bar{h}0l$ is more sensitive and shows both the SF2→SF3 and SF3→SF4 transitions at about 4.5 and 5.5 T clearly. At $H=4.6$ T the temperature variations of the components h and l of the wave vector show a sharp decrease at about $T=3.3$ K corresponding to the SF2→SF3 phase transition but the SF3→SF4 transition has no drastic effect on these wave-vector components. Remembering that SF2 is a commensurate phase with the wave vector $(-1,0,\frac{1}{4})$, Figs. 3(b) and 3(c) illustrate the lock-in transition from the incommensurate SF3 to the commensurate SF2 phase. The nonlinear temperature variations of the components of the wave vector are very similar to the soliton-lattice behavior of the wave vector of the zero-field incommensurate IC phase as it undergoes the lock-in transition to the commensurate AF1 phase.[3]

We have redetermined the magnetic structure of the SF4 phase of $EuAs_3$ at $T=6.0$ K and $H=4.0$ T. The wave vector is found to be $(-0.898,0,0.213)$. Refinement of the magnetic structure with 31 independent reflections (corrected for absorption) gave an agreement factor $R=0.13$. The magnetic moments are modulated collinearly and are oriented at an angle 8° from the crystallographic c axis (see Table I). The amplitude of the magnetic moment is found to be $4.6\mu_B$. Bauhofer *et al.*[5] have determined the magnetic structure of this phase at $T=7$ K and $H=4$ T and have obtained almost identical results.

V. FIELD-INDUCED MAGNETIC PHASES OF ARSENIC-RICH $Eu(As_{1-x}P_x)_3$

The magnetic (H,T) phase diagrams of $EuAs_3$ and arsenic-rich $Eu(As_{1-x}P_x)_3$ are very similar. These phase

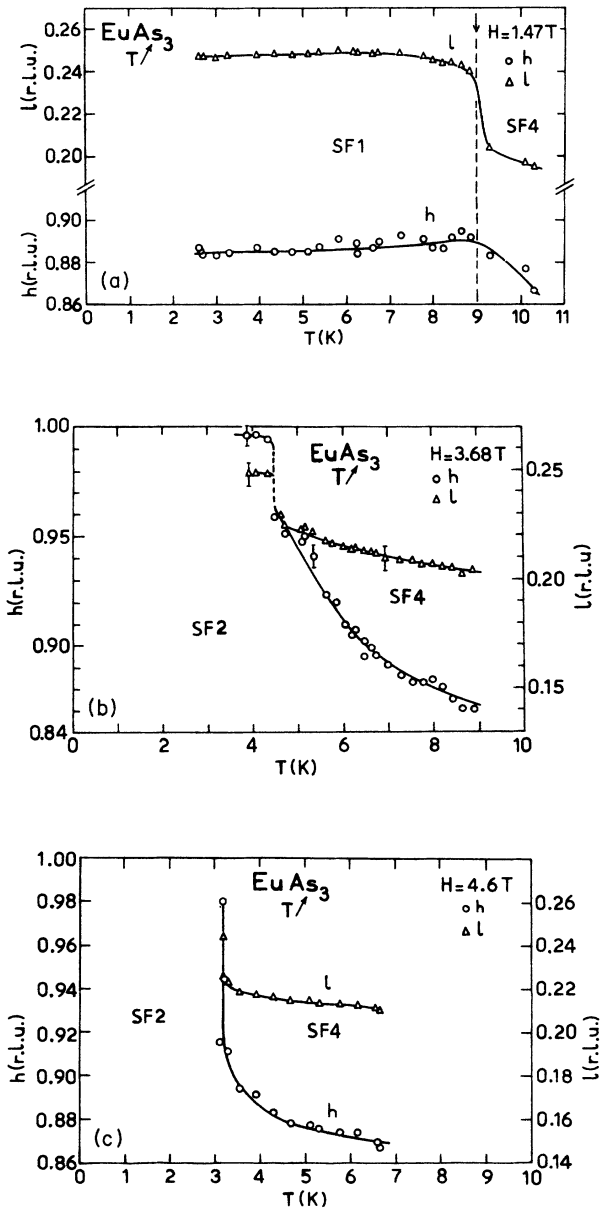

FIG. 3. Temperature variation of the components h and l of the wave vector parallel to $\mathbf{a}^*$ and $\mathbf{c}^*$, respectively, of $EuAs_3$ at (a) $H=1.47$ T; (b) $H=3.68$ T; and (c) $H=4.6$ T. The units for h and l are reciprocal lattice units (r.l.u.). The magnetic field was applied parallel to $\mathbf{b}$. These wave-vector variations illustrate the SF1→SF4 and SF2→SF3→SF4 transitions.

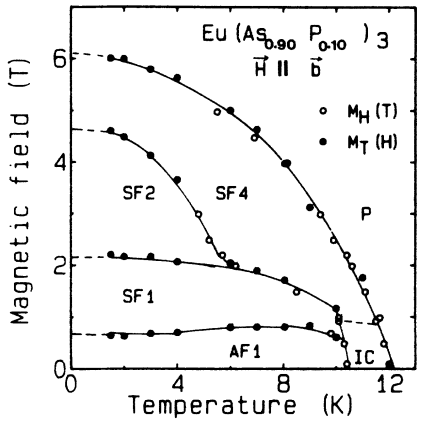

FIG. 4. The magnetic (H,T) phase diagram of $Eu(As_{0.90}P_{0.10})_3$ obtained from magnetization (Ref. 8) and neutron diffraction with the magnetic field applied parallel to the monoclinic b axis of the crystal.

diagrams have already been determined from the magnetization experiments[4,8] for $x=0.10$ and 0.40. Figure 4 shows the magnetic (H,T) phase diagram of $Eu(As_{0.90}P_{0.10})_3$; it is very similar to that of $EuAs_3$ except for the field-induced SF3 phase. We have studied the (H,T) phase diagram of $Eu(As_{0.90}P_{0.10})_3$ using neutron diffraction and found it to agree well with that obtained from magnetization results. We have studied the effect of magnetic field on the incommensurate (IC) phase of $Eu(As_{0.90}P_{0.10})_3$ which could not be obtained from the magnetization measurements. Figure 5 shows the field variation of the components h and l of the wave vector parallel, respectively, to the a^* and c^* axes of the incommensurate IC phase at $T=10.1$ K. In the same figure, field variation of the intensity of the incommensurate satellite reflection is also shown. At about $H=0.92$ T we observe a transition from the incommensurate IC phase to the spin-flop SF4 phase. This spin-flop transition is similar to that observed in $EuAs_3$.

Figure 6 shows the temperature variation of the compounds h and l of the wave vector parallel to a* and c*,

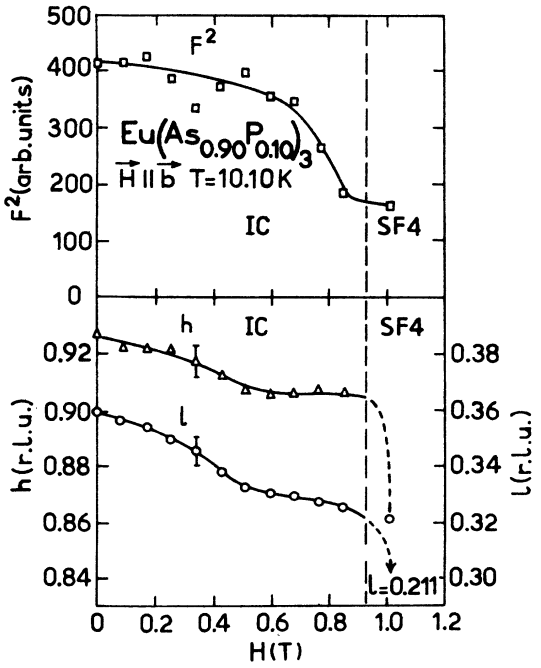

FIG. 5. Field variation of the intensity and the h and l components of the wave vector parallel to $\mathbf{a}^*$ and $\mathbf{c}^*$, respectively, at $T=10.10$ K of $Eu(As_{0.90}P_{0.10})_3$ illustrating field-induced IC→SF4 transition.

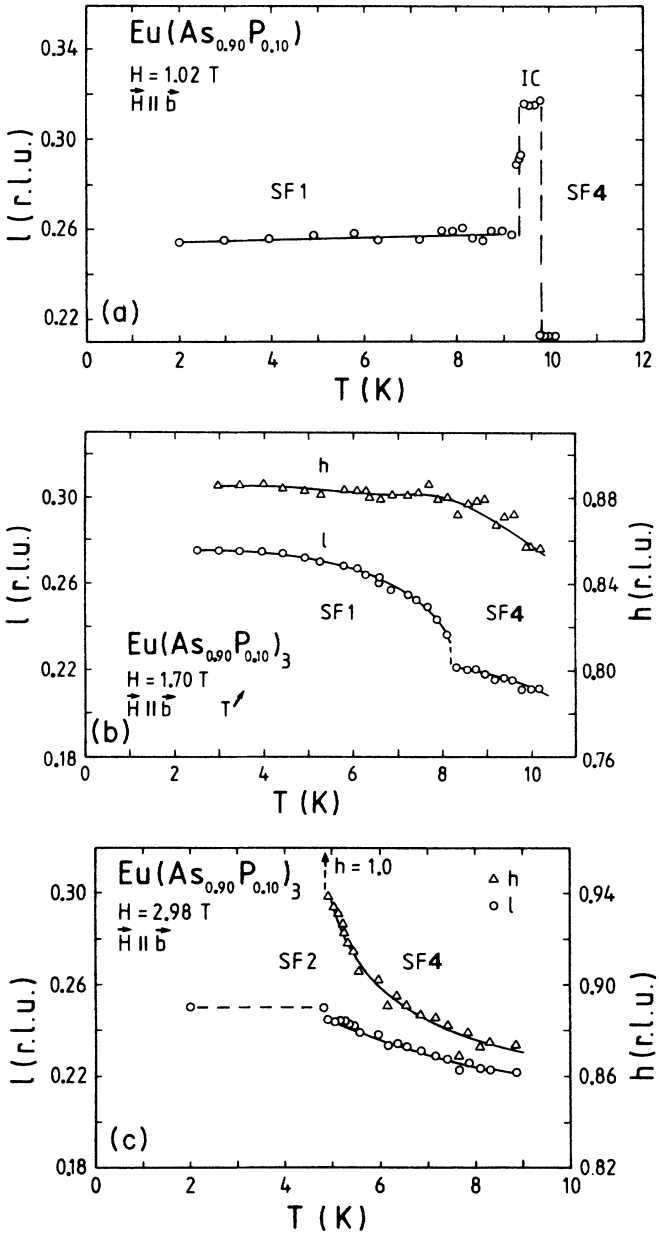

FIG. 6. Temperature variation of the components h and l of the wave vector parallel to $\mathbf{a}^*$ and $\mathbf{c}^*$, respectively, of $Eu(As_{0.90}P_{0.10})_3$ at (a) $H=1.02$ T, (b) $H=1.70$ T, and (c) $H=2.98$ T. The magnetic field was applied parallel to $\mathbf{b}$. These wave-vector variations illustrate SF1→SF4 and SF2→SF4 phase transitions.

respectively, of $Eu(As_{0.90}P_{0.10})_3$ at $H=1.02$, 1.70, and 2.98 T applied parallel to the b axis. These temperature variations of the components of the wave vector show SF1→IC→SF4 transition at $H=1.02$ T, SF1→SF4 transition at $H=1.70$ T and SF2→SF4 transition at $H=2.98$ T by abrupt or continuous charges of the wave-vector components. At $H=2.98$ T the wave-vector variation illustrates the lock-in transition from the incommensurate SF4 phase to the commensurate SF2 phase with the wave vector $(-1,0,\frac{1}{4})$. This wave-vector variation at the lock-in transition is very similar to the soliton-lattice behavior observed for the zero-field incommensurate IC phase of $EuAs_3$ and also that of $Eu(As_{0.90}P_{0.10})_3$.

Figure 7 shows the magnetic (H,T) phase diagram of $Eu(As_{0.60}P_{0.40})_3$ obtained from the magnetization experiments.[4] This phase diagram is also very similar to that of $EuAs_3$ except that, like $Eu(As_{0.90}P_{0.10})_3$, $Eu(As_{0.60}P_{0.40})_3$ has only three field-induced phases compared to the four field-induced magnetic phases of $EuAs_3$. We have determined the magnetic structures of all these three phases, SF-M1, SF-M2, and SF-M4, and the results are given in Table II.

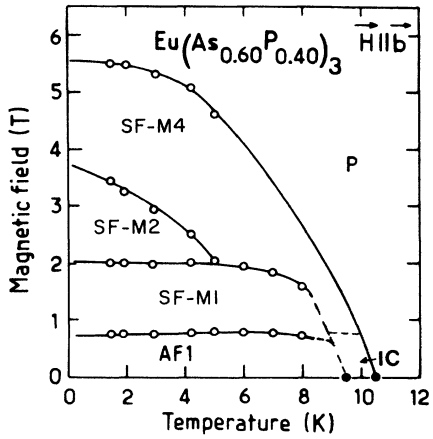

FIG. 7. The magnetic (H,T) phase diagram of $Eu(As_{0.60}P_{0.40})_3$ obtained from magnetization (Ref. 8) and neutron diffraction with the magnetic field applied parallel to the monoclinic b axis of the crystal.

VI. FIELD-INDUCED MAGNETIC PHASES OF PHOSPHORUS-RICH $Eu(As_{1-x}P_x)_3$

The magnetic ordering of phosphorus-rich $Eu(As_{1-x}P_x)_3$ is very different from that in $EuAs_3$ and arsenic-rich $Eu(As_{1-x}P_x)_3$. Magnetic (H,T) phase diagrams of the phosphorus-rich $Eu(As_{1-x}P_x)_3$ have been determined for $x=0.80$ and 0.98 from magnetization experiments.[4,8] Figure 8 shows that of $Eu(As_{0.20}P_{0.80})_3$. The magnetic structures of the field-induced phases are presumably identical or at least similar to those of $Eu(As_{0.02}P_{0.98})_3$. We have only determined the magnetic structures of the field-induced phases in $Eu(As_{0.02}P_{0.98})_3$. For $Eu(As_{0.20}P_{0.80})_3$ we have determined the wave-vector variations as functions of the temperature and the applied magnetic field parallel to **b**. Figure 9 shows the temperature variation of the component l of the wave vector at $H=1.02$, 1.45, and 1.79 T. The component h does not change significantly with temperature and magnetic field and is about 0.78. At $H=1.02$ and at $T=1.5$ K, $l\simeq 0.267$ and remains approximately the same up to $T=5$ K. At higher temperature l decreases continuously. This decrease in l is due to the IC-P1→SF-P2 transition. At $H=1.79$ T, $l=0.27$ and remains constant up to about $T=3.5$ K. At higher temperatures l decreases continuously. This decrease in l is due to the SF-P1→SF-P2 phase transition. At zero applied magnetic field $Eu(As_{0.20}P_{0.80})_3$ orders at $T_N=8.9$ K to an incommensurate sine-wave phase (IC-P2) which instead of undergoing lock-in transition transforms at $T=7.65$ K to a helimagnetic phase (IC-P1).[9] We have determined the effect of magnetic field on the sine-wave phase at $T=7.92$ K. Figure 10 shows the temperature variation of the square of the structure factor of the satellite 0.815,0,0.301 reflection as a function of the applied magnetic field. A second-order phase transition takes place at a critical field $H_c=0.77$ T to the paramagnetic phase. This is consistent with the magnetic (H,T) phase diagram obtained from magnetization experiments. We also determined the effect of the magnetic field applied parallel to **b** on the wave vector $(-0.790,0,0.250)$ of the low-temperature helimagnetic phase IC-P1 of $Eu(As_{0.20}P_{0.80})_3$. The component h of the wave vector does not change significantly with the magnetic field whereas the component l changes with the field. Figure 11 shows the field variation of l at $T=2.0$ K. l increases from $l=0.25$ at $H=0$ to $l\simeq 0.27$ at about $H=1.7$ T. At higher field l decreases, at $H=2.4$ T l is about 0.24. The field variation of l does not show the IC-P1→SF-P1 and SF-P1→SF-P2 transitions clearly but

TABLE II. The magnetic structures of the field-induced phases of $Eu(As_{1-x}P_x)_3$. α is the angle between $\mathbf{a}^*$ axis and the major axis $\mathbf{S}_x$ of the ellipse. S_x and S_y are the components of the magnetic moments along the major and minor axes, respectively. N is the number of independent reflections and R is the agreement factor between the observed and calculated structure factors.

Compound	Phase	T (K)	H (T)	Wave vector	α (deg)	S_x (μ_B)	S_y (μ_B)	N	R
$Eu(As_{0.60}P_{0.40})_3$	SF-M1	2.5	1.15	(−0.894,0,0.315)	100(2)	6.5(4)	2.9(4)	11	0.08
$Eu(As_{0.60}P_{0.40})_3$	SF-M2	2.5	2.07	$(-1,0,\frac{1}{2})$	97.6(7)	5.3(4)		120	0.15
$Eu(As_{0.60}P_{0.49})_3$	SF-M4	2.5	3.22	(−0.912,0,0.323)	99(1)	5.1(4)		11	0.07
$Eu(As_{0.02}P_{0.98})_3$	SF-P1	2.5	1.15	(−0.680,0,0.342)	105(4)	6.3(2)	5.1(3)	81	0.15
$Eu(As_{0.02}P_{0.98})_3$	SF-P2	2.5	1.61	(−0.713,0,0.208)	97(1)	4.4(2)		75	0.22

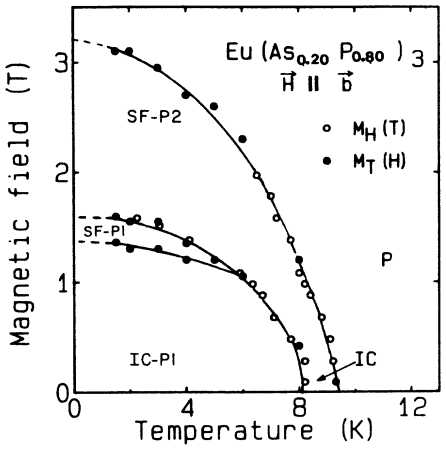

FIG. 8. The magnetic (H,T) phase diagram of $Eu(As_{0.20}P_{0.80})_3$ obtained from magnetization (Ref. 8) and neutron diffraction with the magnetic field applied parallel to the monoclinic b axis of the crystal.

is consistent with the (H,T) phase diagram obtained from the magnetization experiments. However, the field variation of the wave vector at $T=2.0$ K has revealed another interesting effect. Figure 12 shows the ω scans of the satellite reflections as a function of the applied magnetic field $\mathbf{H}\|\mathbf{b}$ at $T=2$ K. The full width at half maximum (FWHM) of the peak at $H=0$ T corresponds to the instrument resolution. The peak becomes increasingly broader as the magnetic field is raised. The shift of the peak to the higher ω values at higher field up to $H=1.5$ T corresponds to the increase in l. At still higher magnetic field the peak position comes back almost to the ω value at $H=0$ corresponding to a decrease in l as is also illustrated in Fig. 11. The field variation of FWHM of these peaks are shown in Fig. 13. At $H=2.4$ T, FWHM$=1.7°$, whereas at $H=0$, FWHM is about 0.7°. This increase in FWHM at $H=2.4$ T by a factor of about 2.4 is very surprising and indicates drastic decrease in the magnetic correlation length. It is a reversible effect—the original FWHM value is retained if the field is reduced to zero. The microscopic origin of this effect is not understood at this time. This behavior of the magnetic peak widths has only been observed in $Eu(As_{1-x}P_x)_3$ with $x=0.80$.

Figure 14 shows the magnetic (H,T) phase diagram of $Eu(As_{0.02}P_{0.98})_3$ obtained from the magnetization experiments.[4] There are only two field induced magnetic phases SF-P1 and SF-P2. The magnetic structures of both these phases are given in Table II.

VII. DISCUSSION

A. Magnetic phase diagrams of $EuAs_3$ and $Eu(As_{1-x}P_x)_3$

The present experimental results demonstrate that the magnetic phase diagrams of the semimetallic $EuAs_3$ and $Eu(As_{1-x}P_x)_3$ ($x \leq 0.98$) are much more complex than is expected for a single Eu^{2+} ion in $^8S_{7/2}$ ground state. The semiconductor β-EuP_3, on the other hand, has a simple classical magnetic phase diagram which is exactly what one expects for a single Eu^{2+} ion.[4]

The magnetic (H,T) phase diagram of $EuAs_3$ has at least two commensurate and four incommensurate phases. The phase boundaries have been determined by the magnetization[4] and by the present neutron diffraction experiments which agree satisfactorily. The magnetic

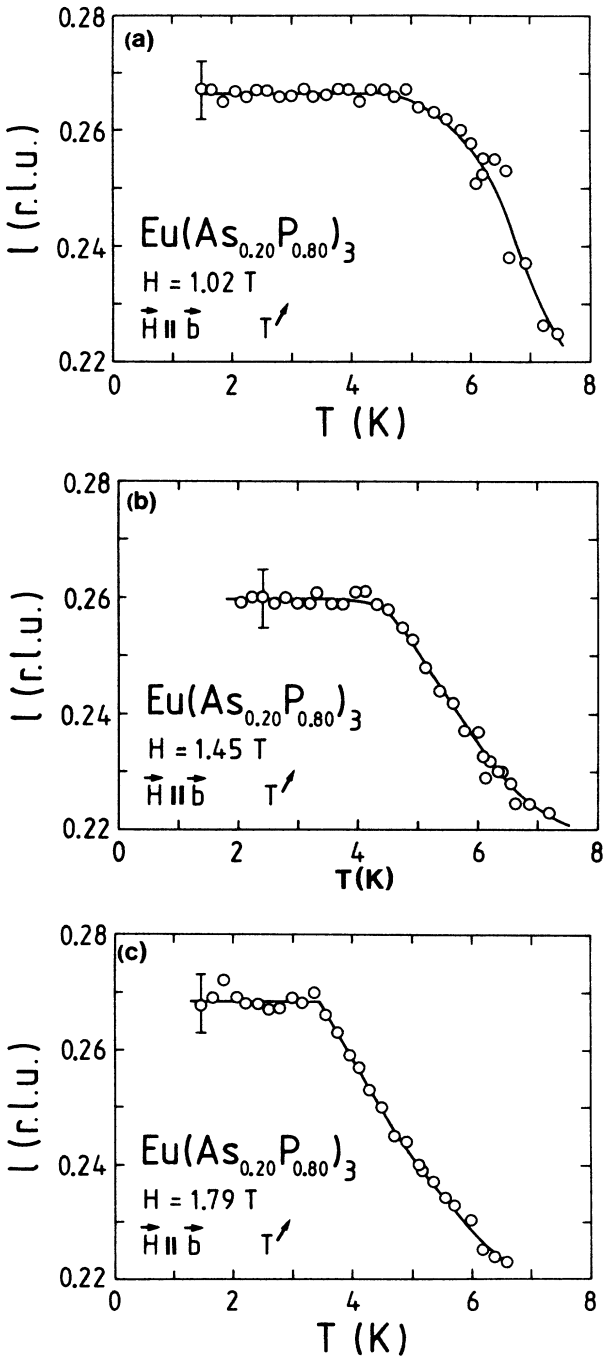

FIG. 9. Temperature variation of the component l of the wave vector parallel to c^* of $Eu(As_{0.02}P_{0.80})_3$ at (a) $H=1.02$ T; (b) $H=1.45$ T; and (c) $H=1.79$ T.

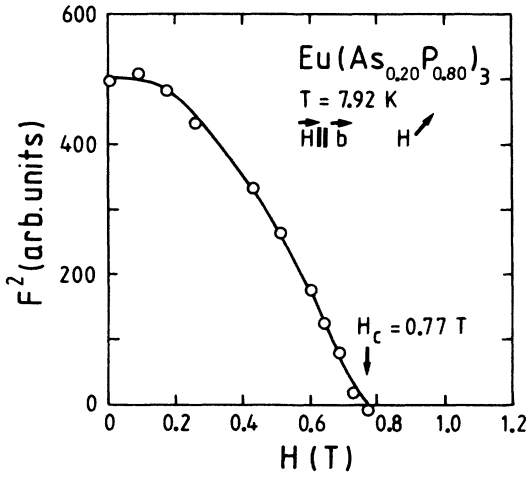

FIG. 10. Field variation of the intensity of the satellite $-0.80,0,0.30$ corresponding to the incommensurate IC-P2 phase of $Eu(As_{0.20}P_{0.80})_3$ illustrating a second-order phase transition to the paramagnetic P phase.

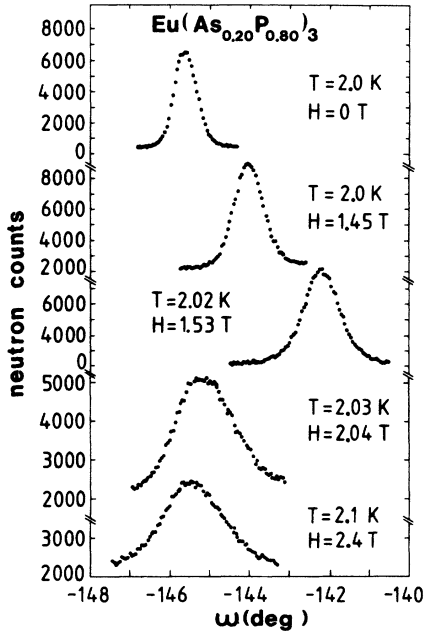

FIG. 12. Field variation of the ω scans of the satellite reflection of $Eu(As_{0.20}P_{0.80})_3$ at about $T=2$ K. The magnetic field was applied parallel to the b axis.

structures of these phases have also been determined in the present work. However, the origin of this complex magnetic phase diagram is not understood. To understand the magnetic ordering of $EuAs_3$ even at zero applied magnetic field and the lock-in phase transition (IC-C) one has to involve strong anisotropic magnetic interactions[3] whose microscopic origin is not understood. Nevertheless, the condition for the existence of the incommensurate $EuAs_3$ at zero applied magnetic field has been investigated phenomenologically by varying the exchange interactions.[3] A simple interpretation of the smooth temperature dependence of the modulation wave vector is given in terms of sine-Gordon soliton-lattice model. To understand the origin of the several magnetic field induced commensurate and incommensurate phases of $EuAs_3$ is a formidably difficult task. However, an external magnetic field may be considered formally as first-order anisotropy.[10] Therefore, temperature induced lock-in transition (SF3→SF2) under external magnetic field applied parallel to [010] can be formally understood even for Eu^{2+} in $^8S_{7/2}$ ground state. In fact, the incommensurate-commensurate transitions observed in $EuAs_3$ at 3.7 and 4.6 T (Fig. 3) have close similarities to those in zero applied magnetic field. At $H=4.6$ T the temperature variation of the components h and l of the wave vector have typical soliton-lattice behavior.

The magnetic (H,T) phase diagram of $Eu(As_{0.90}P_{0.10})_3$ looks very much similar to that of $EuAs_3$ except for that

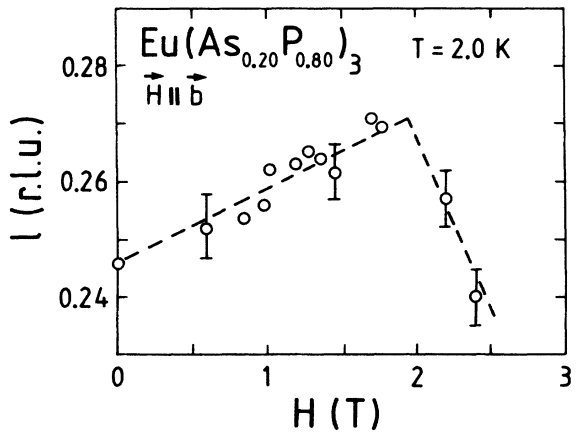

FIG. 11. Field variation of the component l of the wave vector parallel to c^* of $Eu(As_{0.20}P_{0.80})_3$ at $T=2.0$ K with the applied magnetic field parallel to the b axis of the crystal.

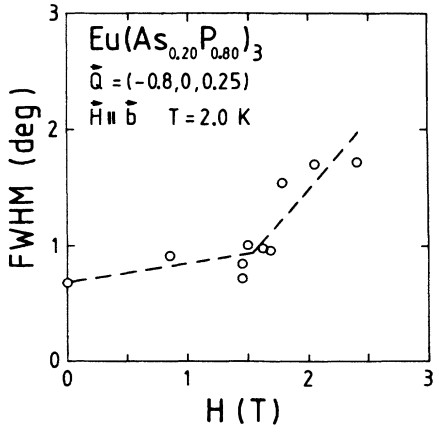

FIG. 13. Field variation of the full width at half maximum (FWHM) of the satellite reflection of $Eu(As_{0.20}P_{0.80})_3$ at $T=2$ K.

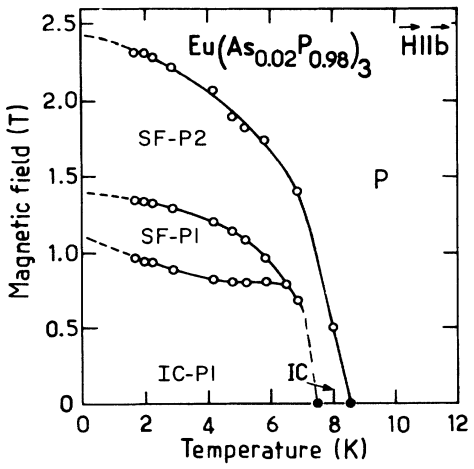

FIG. 14. The magnetic (H,T) phase diagram of $Eu(As_{0.20}P_{0.98})_3$ obtained from magnetization (Ref. 8) and neutron diffraction with the applied magnetic field parallel to the b axis.

in the former compound the phase corresponding to SF3 is missing. The wave vectors and the magnetic structures of all other phases are similar to those of $EuAs_3$. The same is true for $Eu(As_{0.60}P_{0.40})_3$ except for the phase SF-M2. The second field-induced phase SF2 in $EuAs_3$ and $Eu(As_{0.90}P_{0.10})_3$ is a commensurate phase with the wave vector $(-1,0,\frac{1}{4})$ whereas the second field-induced phase in $Eu(As_{0.60}P_{0.40})_3$ is also a commensurate phase but with the wave vector $(-1,0,\frac{1}{2})$. Figure 15 shows the projection of the magnetic structure of the SF-M2 phase of $Eu(As_{0.60}P_{0.40})_3$ along the [010] direction. This phase has the same wave vector as that of the zero-field AF1 phase and also consists of the $(+\ -)$ stacking of the ferromagnetic $(\bar{2}01)$ planes. However, the antiferromagnetic components of the magnetic moments of Eu atoms in SF-M2 phase lie collinearly on the (010) plane and make an angle $\alpha=98°$ with respect to the a^* axis. In the same figure we show the magnetic structures of the other two field-induced phases SF-M1 and SF-M4 of $Eu(As_{0.60}P_{0.40})_3$ which are essentially the same as those of SF1 and SF4 phases of $EuAs_3$.

The magnetic phase diagrams of the phosphorus rich $Eu(As_{0.20}P_{0.80})_3$ and $Eu(As_{0.02}P_{0.98})_3$ contain only four magnetic phases. At zero field these compounds order at about $T_N=8.5$ K to a sine-wave incommensurate phase with the magnetic moments parallel to $\pm\mathbf{b}$. At about 1 K below T_N this sine-wave phase IC undergoes a first-order phase transition to a helimagnetic phase IC-P1 in which the magnetic moments are modulated in the (010) plane. This phase is similar to the antiferromagnetic component of the SF1 phase of $EuAs_3$. Application of magnetic field induces two other phases SF-P1 and SF-P2. Figure 16 shows the projection of the magnetic structures of IC-P1, SF-P1 and SF-P2 phases along [010]. SF-P2 is very similar to the SF4 phase of $EuAs_3$. SF-P1 is actually an incommensurate phase with the wave vector $(-0.680,0,0.342)$. However, looking at Fig. 16 we observe that this phase is nearly commensurate with the wave vector $(-\frac{2}{3}0\frac{1}{3})$. It consists of ferromagnetic (-201) planes stacked in the sequence $(+\searrow\swarrow-)$. The spin directions in the neighboring plane are rotated by 120°.

Figure 17 shows the resulting (H,x) phase diagram of $Eu(As_{1-x}P_x)_3$ at $T=1.8$ K. This phase diagram is not complete and the concentration range $0.40<x<0.80$ remains uninvestigated. However, since the magnetic structures of the phases of $Eu(As_{1-x}P_x)_3$ have been determined for $x=0.40$ and 0.98, we are in a position to comment on the general features of this phase diagram. The low-temperature and low-field antiferromagnetic phase AF1 disappears for x in between 0.40 and 0.80 and instead a helimagnetic phase IC-P1 is stabilized. This phase is almost identical to the first field-induced SF1 phase of $EuAs_3$. At intermediate field we have a series of commensurate phases SF2, SF-M2, and a nearly commensurate SF-P1 phase. At higher fields we have SF4 phase for arsenic-rich $Eu(As_{1-x}P_x)_3$ and SF-P2 phase for phosphorus-rich $Eu(As_{1-x}P_x)_3$. We have already mentioned that these two phases are nearly identical. We

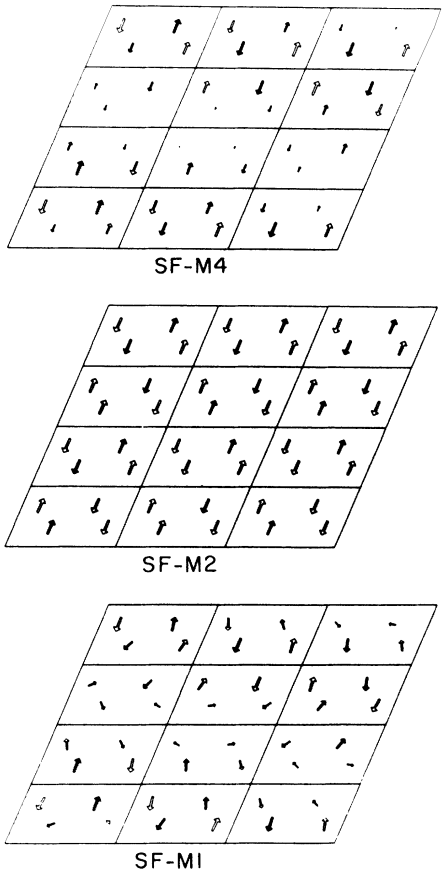

FIG. 15. Projection of the magnetic structures of the field-induced SF-M1, SF-M2, and SF-M4 phases of $Eu(As_{0.60}P_{0.40})_3$. The europium atoms which are at $z=\frac{1}{2}$ are shown by shaded arrows.

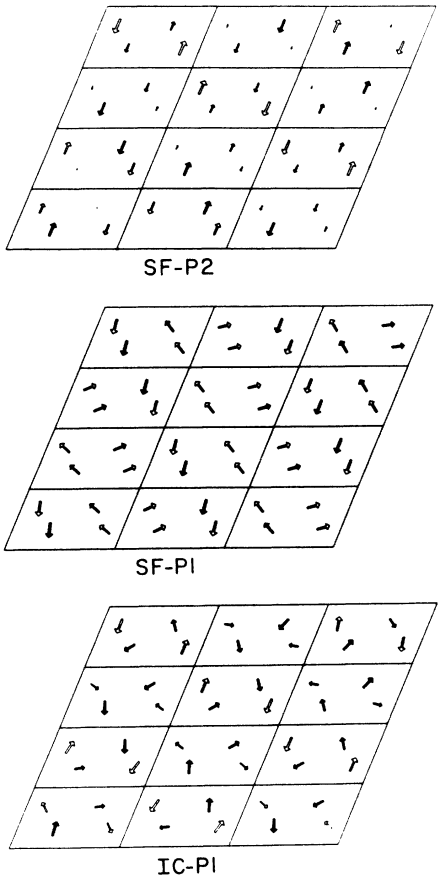

FIG. 16. Projection of the magnetic structures of the field-induced IC-P1, SF-P1, and SF-P2 phases of $Eu(As_{0.02}P_{0.98})_3$. The europium atoms which are at $z=\frac{1}{2}$ are shown by shaded arrows.

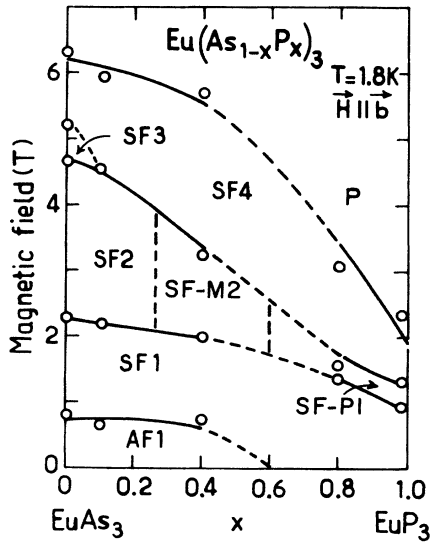

FIG. 17. (H,x) phase diagram of $Eu(As_{1-x}P_x)_3$.

note that the critical field necessary for the transition to the paramagnetic phase reduces drastically from about 6.3 T for $EuAs_3$ ($x=0$) to about 2.3 T for $x=0.98$.

B. Sine-wave phases of $EuAs_3$ and $Eu(As_{1-x}P_x)_3$

The magnetic structure of the high-field phases SF4, SF-M4, and SF-P2 (these are actually the same phase) is found to be a sine-wave modulated phase with the magnetic moments oriented approximately along the c axis. We have determined these structures of SF4, SF-M4, and SF-P2 phases at 4, 2.5, and 2.5 K, respectively. Structure refinements with the elliptic spiral model (see Sec. III) lead to the axial ratio $\gamma=S_y/S_x\simeq 0$ suggesting these structures to be actually sine-wave at these temperatures. Structure refinements have been performed at temperatures considerably lower than T_N (for example, for SF-M4 the structure refinement has been performed at $T=2.5$ K, $H=3.2$ T, and $T_N\simeq 9$ K at this magnetic field). At T_N the development of the sine-wave modulation can be understood by considering mainly the second-order terms of the free energy. However, as the temperature is decreased fourth-order or higher-order terms can become important.[11] These higher-order terms may have an entropic origin for the magnetic moments tend to saturate at low temperatures or these may be in general due to single-ion anisotropy or higher-order exchange interactions like quadrupolar interactions. These higher-order terms can be classified into two categories.[11] The first category contains the so-called locking terms, which give rise to the shift of the wave vector towards a commensurate value leading to a lock-in transition. This lock-in transition has been observed in $EuAs_3$ and $Eu(As_{1-x}P_x)_3$ at zero and low magnetic field. The second category of higher-order terms contains terms that introduce a coupling with another Fourier component leading to the appearance of third-, fifth-, and higher-order harmonics in addition to the principal satellite in the diffraction picture. This behavior is typical of the sine-wave modulations which become progressively square-wave-type with decreasing temperature. Unfortunately, in our present experiments we have not investigated the higher-order harmonics of the high-field phases of $EuAs_3$ and $Eu(As_{1-x}P_x)_3$ and therefore we cannot make definite conclusions regarding whether the sine-wave high-field phases actually transform progressively to a square-wave modulation or remain actually sine-wave down to low temperatures.

We observe that the first magnetic phase at T_N in $EuAs_3$ and $Eu(As_{1-x}P_x)_3$ is always a sine-wave modulation. At zero applied magnetic field the sine-wave modulation is transverse, i.e., the magnetic moments are aligned perpendicular to the wave vector direction. At higher magnetic fields the antiferromagnetic component of the magnetic structure is also sine-wave but not transverse. This sine-wave phase is not pure longitudinal, but very close to it. Field-induced phase transitions between these two sine-wave phases have been demonstrated for $EuAs_3$ and $Eu(As_{0.90}P_{0.10})_3$ in Figs. 2 and 5, respectively, and actually exist for $Eu(As_{1-x}P_x)$ for all $x\leq 0.98$. A sine-wave magnetic structure can be described within a

one-dimensional representation by the Fourier component m_k:[11]

$$m_k = \frac{A_k}{2}\hat{\mathbf{u}}_k e^{i\phi_k} . \quad (2)$$

The magnetic moment in any elementary unit cell is given by

$$\mathbf{m}_l = A_k \cos(\mathbf{k}\cdot\mathbf{R}_l + \phi_k)\hat{u}_k . \quad (3)$$

Equation (3) describes a sine-wave modulation of the moment value propagating along $\mathbf{k}$ direction with amplitude A_k, polarization along the unit vector $\hat{\mathbf{u}}_k$ and phase ϕ_k. When the crystallographic site has several magnetic atoms, the Fourier component $\mathbf{m}_{kj}$ can be defined for Bravais sublattice j as

$$\mathbf{m}_{k,j} = \frac{A_k}{2}\mathbf{u}_{k,j} e^{i\phi_{k,j}} , \quad (4)$$

where the polarizations $\hat{u}_{kj}$ and the phases ϕ_{kj} are defined by the basis vectors of the irreducible representation $\Gamma_{k\nu}$ of the group $\mathbf{G}_k$, the little group or the group of the wave vector $\mathbf{k}$.[11] When the group $\mathbf{G}_k$ has a high symmetry the sine-wave modulation has to be longitudinal with a polarization parallel to the principal axis. However, when $\mathbf{G}_k$ has lower symmetry, viz., orthorhombic, monoclinic, or triclinic [monoclinic in the case of $EuAs_3$ and $Eu(As_{1-x}P_x)_3$] the sine-wave modulation can be either longitudinal ($\mathbf{m}_k \| \mathbf{k}$) or transverse ($\mathbf{m}_k \perp \mathbf{k}$). A temperature-induced phase transition between the longitudinal and transverse sine-wave has been observed in Cr (Ref. 10) at about 124 K. Field-induced phase transition between these two types of sine-wave phases in $EuAs_3$ and $Eu(As_{1-x}P_x)_3$ is to our knowledge the only other example for such a phase transition.

C. Helimagnetic phases in $EuAs_3$ and $Eu(As_{1-x}P_x)_3$

We have discussed in Sec. VII B that a sine-wave modulation which appears at T_N can either lock into a commensurate phase or transform gradually into a square-wave modulation as the temperature is lowered. Only in special cases can the sine-wave modulation remain stable down to $T=0$ if the ground state is a singlet.[11] There is, however, a fourth possibility in which the sine-wave phase which appears at T_N can transform into a helimagnetic phase as the temperature is lowered. For orthorhombic or lower symmetry, the irreducible representations are only one dimensional and therefore a helimagnetic ordering, for which the order parameter belongs to a two-dimensional irreducible representation, cannot develop at T_N if the phase transition is second order. The incommensurate phase, which develops at T_N, must therefore be a sine-wave modulation. However, as the temperature is lowered a transition to a helimagnetic phase can occur because the helimagnetic phase has a lower energy at low temperatures. This transition can be very close to T_N when isotropic exchange interactions dominate anisotropic ones. This situation seems to be fulfilled in the case of phosphorus-rich $Eu(As_{1-x}P_x)_3$ at zero and low applied magnetic fields. We actually observe such a sine-wave to helimagnetic transition at a tmeperature T which is about 1 K below T_N. The antiferromagnetic component of the field-induced SF1 phase of $EuAs_3$ and $Eu(As_{1-x}P_x)_3$ is actually very similar to the low-temperature helimagnetic phase IC-P1 of the phosphorus-rich $Eu(As_{1-x}P_x)_3$.

VIII. SUMMARY AND CONCLUSIONS

We have determined the magnetic structures of the field-induced phases of $Eu(As_{1-x}P_x)_3$ and have studied the temperature, and magnetic-field-induced phase transitions between these phases by neutron diffraction on single crystals. Temperature and field variations of the wave vectors have been determined carefully. We have discovered several types of novel phase transitions in this system, viz., incommensurate to commensurate lock-in transition, sine-wave to helimagnetic and transverse sine-wave to longitudinal sine-wave phase transitions. The observation of such a variety of commensurate and incommensurate phases and the above-mentioned phase transitions between these are quite unexpected for a single Eu^{2+} ion in the $^8S_{7/2}$ ground state.

From the basis of the present investigations the following conclusions are made.

(1) The semimetallic $EuAs_3$ and $Eu(As_{1-x}P_x)_3$ have very complex magnetic (H,T) phase diagrams which contain several commensurate and incommensurate phases unexpected for a single Eu^{2+} ion in the $^8S_{7/2}$ ground state. The magnetic (H,T) phase diagram of the semiconductor β-EuP_3, on the other hand, is very simple and is exactly what one expects for a S-state Eu^{2+} ion.

(2) The charge carrier concentration in semimetallic $Eu(As_{1-x}P_x)_3$ decreases drastically as the phosphorus concentration increases and pure β-EuP_3 is an insulator at low temperature. The exchange coupling in semimetallic $EuAs_3$ and $Eu(As_{1-x}P_x)_3$ is presumably a combination of superexchange and Ruderman-Kittle-Kasuya-Yosida (RKKY) interaction whereas for β-EuP_3 only the superexchange is important. the complex magnetic properties of the semimetallic $Eu(As_{1-x}P_x)_3$ should therefore be mainly due to the RKKY interaction.

(3) By assuming anisotropic exchange interaction the stabilities of the incommensurate and the commensurate zero-field phases have been understood phenomenologically.[3,7] Similar analysis of the field-induced phases is a formidably difficult task and has not been performed as yet.

(4) Incommensurate-commensurate lock-in transitions have been investigated in $EuAs_3$ and $Eu(As_{1-x}P_x)_3$ at zero field and also with applied magnetic field. The soliton-lattice behavior of the temperature variation of the wave vector has been observed in both cases. However, the higher-order harmonics which should appear theoretically close to the lock-in transition have not been found experimentally.

(5) The highest field-induced SF4 and IC-P2 phases (actually the same phase) are sine-waves phases in which the magnetic moments are oriented approximately parallel to the c axis. This sine-wave phase which appears at T_N should gradually transform to a square-wave modulation.

We have analyzed the magnetic structure at $T=2.5$ K ($T_N \simeq 9$ K) and have found no evidence of squaring up. However, this point deserves further experimental investigation.

(6) We have observed the field-induced transverse sine-wave (TSW) to longitudinal sine-wave (LSW) phase transition. The only other known such phase transition is the temperature-induced LSW $\rightarrow$ TSW transition in Cr.

(7) A sine-wave to helimagnetic phase transition has been observed for the first time in the phosphorus-rich $Eu(As_{1-x}P_x)_3$ at zero applied field.

(8) The commensurate low-temperature antiferromagnetic phase of $Eu(As_{1-x}P_x)_3$ disappears at a concentration x which lie in the uninvestigated range $0.40 < x < 0.80$ and gives rise to a helimagnetic phase for higher phosphorus concentrations.

(9) The critical magnetic field for the transition to the paramagnetic phase of $Eu(As_{1-x}P_x)_3$ decreases drastically from about 6.3 T for $x=0$ to 2.3 T for $x=0.98$. This must be somehow related to the depletion of the charge carrier concentration with increasing x.

(10) As a final conclusion we add that the semimetallic $EuAs_3$ and the solid solutions $Eu(As_{1-x}P_x)_3$ shows magnetic behavior which is as exciting as the cerium monopnictides.[11] The origin of anisotropy in these compounds is not understood at the present state of knowledge. However, the proximity of Eu $4f$ state to the Fermi level in these semimetallic compounds might lead to the p-f hybridization giving rise to anisotropy. More theoretical investigations to understand the magnetic properties of $EuAs_3$ and $Eu(As_{1-x}P_x)_3$ are needed.

ACKNOWLEDGMENTS

We wish to thank Professor H. G. von Schnering for his encouragement and support and Dr. J. Rossat-Mignod for critical discussions. One of us (T.C.) wants to acknowledge the financial support of the Sonderforschungsbereich-125 Aachen-Jülich-Köln. The experiments have been performed at the Institut Laue-Langevin and the facilities provided by this Institute are gratefully acknowledged.

[1]T. Chattopadhyay, H. G. von Schnering, and P. J. Brown, J. Magn. Magn. Mater. **28**, 247 (1982).

[2]W. Bauhofer, T. Chattopadhyay, M. Möllendorf, E. Gmelin, H. G. von Schnering, U. Steigenberger, and P. J. Brown, J. Magn. Magn. Mater. **54-57**, 1359 (1986).

[3]T. Chattopadhyay, P. J. Brown, P. Thalmeier, and H. G. von Schnering, Phys. Rev. Lett. **57**, 372 (1986).

[4]T. Chattopadhyay, H. Bartholin, J. Voiron, W. Bauhofer, and H. G. von Schnering, J. Magn. Magn. Mater. **63&64**, 632 (1987).

[5]W. Bauhofer, U. Steigenberger, and P. J. Brown, J. Magn. Magn. Mater. **67**, 49 (1987).

[6]W. Bauhofer, E. Gmelin, M. Möllendorf, R. Nesper, and H. G. von Schnering, J. Phys. C **18**, 3017 (1985).

[7]T. Chattopadhyay, P. J. Brown, P. Thalmeier, W. Bauhofer, and H. G. von Schnering, Phys. Rev. B **37**, 269 (1988).

[8]T. Chattopadhyay, J. Voiron, and H. Bartholin, J. Magn. Magn. Mater. **72**, 35 (1988).

[9]T. Chattopadhyay, P. J. Brown, and H. G. von Schnering, Phys. Rev. B **36**, 7300 (1987).

[10]Yu. A. Izyumov, Usp. Fiz. Nauk **144**, 439 (1984) [Sov. Phys.—Usp. **27**, 845 (1984)], and references included therein.

[11]J. Rossat-Mignod, in *Neutron Scattering in Condensed Matter*, edited by K. Sköld and D. L. Price (Academic, New York, 1986).